Low temperature sintering of Ba(Zr0.8 − xCexY0.2)O3 − δ using lithium fluoride additive

Authors: C.-L. Tsai, M. Kopczyk, R. J. Smith, and V. Hugo Schmidt

C.-L. Tsai, M. Kopczyk, R.J. Smith, and V.H. Schmidt, "Low temperature sintering of Ba(Zr0.8-xCexY0.2)O 3 - δ using lithium fluoride additive," Solid State Ionics 181, 1083-1090 (2010). doi: 10.1016/j.ssi.2010.06.028.

Low temperature sintering of $Ba(Zr_{0.8-x}Ce_xY_{0.2})O_{3-\delta}$ using lithium fluoride additive

C.-L. Tsai *, M. Kopczyk, R.J. Smith, V.H. Schmidt

Department of Physics, Montana State University, Bozeman, MT 59717, USA

A B S T R A C T

Lithium fluoride (LiF) was selected as a liquid phase sintering additive to lower the sintering temperature. The effects of LiF on the sinterability, microstructure, and electrochemical properties of $Ba(Zr_{0.8-x}Ce_xY_{0.2})O_{3-\delta}$ ($0 \le x \le 0.4$) (BZCYs) ceramics were investigated. Using LiF as an additive, high density BZCYs ceramics can be obtained at sintering temperatures 200–300 °C lower than the usual 1700 °C with much shorter soaking time. Nuclear reaction investigations showed no lithium and a small amount of fluorine reside in the sample which indicates the non-concomitant evaporation of lithium and fluorine during the sintering process. Scanning electron microscopic investigations showed the bimodal structure of BZCYs ceramics and grain growth as Ce content increases. In a water saturated hydrogen containing atmosphere, BZCYs ceramics have higher conductivity when LiF is used in the sintering process. LiF-added BZCYs electrolyte-supported fuel cells with platinum electrodes were tested at temperatures from 500 to 850 °C. Results show that LiF is an excellent sintering additive for lowering the sintering temperature of BZCYs.

1. Introduction

Rare-earth-doped perovskite-type oxides based on $BaCeO_3$, $BaZrO_3$, $SrCeO_3$ and $SrZrO_3$ have attracted a lot of attention due to their high proton conductivities under hydrogen or steam containing atmospheres at elevated temperature. This type of material has potential for applications such as hydrogen separation membranes, hydrogen pumps, hydrogen sensors and electrolytes for fuel cells [1–3]. The introduction of trivalent dopant into the perovskite structure leads to the creation of oxygen vacancies as shown in Eq. (1), e.g. Y-doped $BaCeO_3$ (Kroeger–Vink notation)

$$2Ce_{Ce}^{x} + O_O^x + Y_2O_3 \rightarrow 2Y_{Ce}^{'} + V_O^{\bullet\bullet} + 2CeO_2. \quad (1)$$

When exposing to steam or hydrogen containing atmospheres, hydroxide species can be produced as shown in Eqs. (2) and (3)

$$H_2O_{(g)} + O_O^x + V_O^{\bullet\bullet} \rightarrow 2OH_O^{\bullet} \quad (2)$$

$$\frac{1}{2}H_2 + O_O^x \rightarrow OH_O^{\bullet} + e^{'}. \quad (3)$$

The protons inside the material can migrate freely from one oxygen ion to a neighboring one which results in high proton conductivity [3].

Among the high temperature proton conductors, Y-doped barium cerate (BCY) shows the highest proton conductivity but it tends to decompose into proton insulating barium carbonate ($BaCO_3$) or barium hydroxide ($Ba(OH)_2$) and cerium oxide (CeO_2) when exposed to a CO_2 or H_2O containing atmosphere [4–9]. In contrast to BCY, Y-doped barium zirconate (BZY) shows high chemical stability but has relatively low proton conductivity due to its high proton resistance at grain boundaries [10–13]. Since a solid solution can be formed easily between barium cerate and barium zirconate, it is possible to find a composition for a compromise between high proton conductivity and high chemical stability. From this point of view, C.-S. Tu et al., Z. Zhong and E. Fabbri et al. studied the stability and conductivity of Ce-substituted Y-doped barium zirconate [14–17]. K. H. Ryu et al. investigated the stability and conductivity of Gd- and Nd-doped Ce-substituted Y-doped barium zirconate [18].

In the fabrication process, one of the major challenges is that the material is hard to sinter to high density (>93%) which is required for the electrolyte membrane of SOFCs. Usually, extreme temperature (1700 °C–1800 °C), long soaking times (>20 h) and fine powders are required for producing high density BZY. Although BCY is easier to sinter, it still requires temperature higher than 1600 °C and more than 10 h to get a high density pellet. Under this extreme condition, not only is economic efficiency low but it also causes barium evaporation which results in low conductivity [4,9,18]. Different methods have been used to attack this problem which includes using wet chemical methods to produce fine powders and using ZnO as a sintering additive to reduce the sintering temperature [10,19–21]. However, the improvement from using wet chemical methods is limited and the introducing of ZnO results in a Zn evaporation problem at temperature higher than 1300 °C which results in dropping more than 20% of relative density when sintering temperature is higher than 1300 °C. This Zn evaporation problem may cause a problem when a long

working time at high temperature is needed for the device. Moreover, Zn can actually replace the element at the B-site and change the microstructure which results in lowering the conductivity.

Li^+ is an easily diffusing ion at low temperature which makes it a very efficient sintering additive for many perovskite materials. The addition of lithium in a form such as lithium fluoride (LiF), has been used to sinter $BaTiO_3$ and $CaZrO_3$ at a temperature of 250–300 °C lower than that necessary for pure material densification [22–24]. The aim of the work described in this paper was to densify $Ba(Zr_{0.8-x}Ce_xY_{0.2})O_{3-\delta}$ ($0 \le x \le 0.4$) ceramics by introducing lithium fluoride and to study the corresponding microstructures and electrochemical properties. The densified ceramics were then examined by testing them at fuel cell operating conditions. For convenience, we denote BZCYs, BZY82, BZCY712, BZCY622, BZCY532, BZCY442 and BZCYs/LiF to represent $Ba(Zr_{0.8-x}Ce_xY_{0.2})O_{3-\delta}$ ($0 \le x \le 0.4$), $Ba(Zr_{0.8}Y_{0.2})O_{2.9}$, $Ba(Zr_{0.7}Ce_{0.1}Y_{0.2})O_{2.9}$, $Ba(Zr_{0.6}Ce_{0.2}Y_{0.2})O_{2.9}$, $Ba(Zr_{0.5}Ce_{0.3}Y_{0.2})O_{2.9}$, $Ba(Zr_{0.4}Ce_{0.4}Y_{0.2})O_{2.9}$ and $Ba(Zr_{0.8-x}Ce_xY_{0.2})O_{3-\delta}$ ($0 \le x \le 0.4$) mixed with LiF sintering additive, respectively.

2. Experimental procedures

2.1. Preparation of BZCY powders

BZCY powders were synthesized by the Glycine-Nitrate Process. Barium nitrate ($Ba(NO_3)_2$, 99.999%), zirconium dinitrate oxide hydrate ($ZrO(NO_3)_2 \cdot xH_2O$, 99.9%), cerium nitrate hexahydrate ($Ce(NO_3)_3 \cdot 6H_2O$, 99.5%) and yttrium nitrate hexahydrate ($Y(NO_3)_3 \cdot 6H_2O$, 99.9%) purchased from Alfa Aesar were dissolved in distilled water. Stoichiometric amount of solutions were weighed and mixed. In addition to constituents, 1.8 times the number of Ba moles of Glycine were added to and dissolved in the solution. The solutions were heated on a hot plate under stirring until precipitations were seen and then cooked by a stove to get a viscous gel, then auto-ignited to form powders. The powders were collected and calcined at a temperature of 1400 °C for 2 h to remove possible carbon and impurity residues and form well-crystallized BZCYs. X-ray diffraction (Scintag, XGEN-400) with Cu Kα ($\lambda = 1.5418$ Å) was used to confirm the single phase of each calcined powder. After the confirmation of single phase BZCYs, powders with and without 7 wt.% LiF were planetary ball milled with yttrium stabilized zirconia ball media and ethanol at 150 rpm for 4 h. The solutions were dried and pressed into discs by using a die press. The 6.36 mm diameter discs for dilatometric measurements were pressed under a load of 1.5 tons. The 12 mm diameter discs for the sintering studies were pressed under a load of 5 tons.

2.2. Densification studies

Densification studies were performed by measuring linear shrinkage from dilatometry and direct measurements of density were made from the sintered samples. Dilatometric measurements were carried out in static lab air using a Linseis Dilatometer L75. All of the measurements were made with 3 °C/min heating rate from room temperature up to 1500 °C. Sintering studies were done at temperatures between 1100 °C and 1500 °C with different dwell time in a static air atmosphere. To prevent Ba evaporation at high temperature, samples were covered by the same powder during the sintering process. Densities of sintered samples were measured by the Archimedes method using pure ethanol as the immersion medium.

2.3. LiF detection

A series of BZCY622/LiF samples sintered at 1400 °C, using 5 K/min heating and 10 K/min cooling, with different dwell times were used in this investigation. After polishing one side of the samples to the midplane of their original thickness, a 2 MeV Van de Graaff linear accelerator capable of producing a proton beam current of up to 1 μA was used to carry out a nuclear reaction process. A silicon surface barrier detector was placed at an angle of 150° relative to the incident particle beam path and used to detect alpha particles resulting from the nuclear reactions:

$$^7Li + p \rightarrow {}^4He + \alpha \quad (4)$$

$$^{19}F + p \rightarrow {}^{16}O + \alpha. \quad (5)$$

SIMNRA software by Matej Mayer was then used to simulate the experiment data and integrate the alpha particle spectra peaks to determine the amount of lithium and fluorine residing in the samples.

2.4. Microstructure study

The microstructures of sintered samples were investigated by Field Emission Scanning Electron Microscopy (SUPRA™ 55 Versatile High Performance FESEM, Zeiss). Before the study, the samples for investigation were polished by diamond sand paper to remove any possible impurities on the surface. Thermal etching was then applied in order to see the grain interiors and grain boundaries.

2.5. Electrochemical study

Electrochemical impedance data collections were carried out using a Solartron 1260 impedance analyzer with a 100 mV/cm applied ac field. For comparison, samples sintered at 1400 °C for 5 h with LiF sintering additive and 1500 °C for 10 h without LiF sintering additive were chosen for this study. Before the measurements, both sides of the samples were polished to remove any possible impurities and then brush-painted with silver paint (SPI Flash-Dry Silver Paint) to serve as electrodes. The samples were first fired to 850 °C with 3 °C/min ramp rate and held at 850 °C for 5 h to reach equilibrium to ambient atmosphere before measurements were taken. The impedance spectra were obtained in the frequency range of 0.1 Hz to 1 MHz between 850 °C and 75 °C with a 25 °C step in a water saturated ($P_{H2O} = 3.5$ kPa) 4% H_2/96% Ar atmosphere. ZView (Scribner Associates, Inc.) electrochemical impedance software was used for data analysis. At high temperature, ~400 °C and higher, the experiment encountered a limitation, that either the bulk arc or the grain boundary arc was no longer accessible, because the characteristic frequency exceeded the measuring ability of our equipment. Therefore, the intersection value between the Z′ axis and the data was taken as the total resistance of the sample.

2.6. Cell fabrication and test

BZCYs powders with 7 wt.% LiF were pressed into 32 mm diameter pellets using a uniaxial die press under a load of 8 tons and sintered at 1400 °C for 5 h. The pellets were then polished down to 300 μm of thickness to serve as electrolytes. Pt paint (SPI-Chem conductive platinum paint) was brush-painted onto BZCYs/LiF electrolytes by hand and then sintered at 1000 °C for 2 h to serve as electrodes. The effective area for all cells was 3.9 cm^2. A homemade seal-less fuel cell testing system was used for testing. Silver mesh and nickel foam were used as cathode and anode current collectors, respectively. Gas flows were controlled by MKS 1179A Elastomer-Sealed Mass Flow Controllers. The flow rate of fuel gas was 100 ml/min of H_2 mixed with 150 ml/min of N_2 and the cathode gas flow rate was 350 ml/min of air. Water vapor concentration in the fuel gas was about 3.5% by flowing fuel gas through a water bubbler at room temperature. For each temperature, cells were kept at open circuit for 20 min, followed by I–V curve measurement for 10 min, next by a 0.5 V test run for 30 min and then cooled to the next temperature.

3. Results and discussion

Fig. 1 shows the XRD patterns of BZCYs/LiF ceramics which were sintered at 1400 °C for 5 h. All samples displayed a single phase without any LiF-related product peak. The XRD spectra shift to lower angle with increasing Ce concentration which results from the substitution of bigger Ce^{+4} (0.87 Å) for smaller Zr^{+4} (0.72 Å) ions at the B-site. The pseudo-cubic lattice parameters calculated from the XRD spectra are shown in Fig. 2. The linearly increasing lattice parameter indicates that Ce atoms are homogeneously distributed inside the barium zirconate structure and reveals the good stoichiometry of the samples.

The differences in sintering behavior between BZCYs/LiF and BZCYs are shown in Fig. 3. Dilatometric results show that BZCYs/LiF started their densification process at ~600 °C while samples without LiF started at ~1000 °C. The sintering behaviors of BZCYs/LiF accelerated right after 600 °C and reached the fastest sintering rate in the whole process between 700 °C and 1000 °C. This high shrinkage rate is correlated to the melting point of LiF at 848 °C, about the central point between 700 °C and 1000 °C. After 1000 °C, the shrinking process slowed down, whereas the BZCYs shrinkage mechanism was introduced at this temperature, as seen in BZCYs' sintering behavior. The total shrinkages of BZCYs/LiF samples were between ~15% and ~20%, depending on the composition, which is about four times that of the BZCYs samples. If we assume that all the LiF evaporated out of the samples during the sintering process, the contribution from LiF evaporation to the shrinkage is about ~5%. After subtracting this factor due to the presence of LiF, the results still give us two to three times of higher shrinkage in samples with LiF than in those without LiF.

A further observation in the sintering study was made on a series of samples sintered in a kiln furnace between 1100 °C and 1500 °C. It was found that dense ceramics (>90%) only result from sintering temperatures higher than 1200 °C; 1100 °C only giving results of ~70% density. Comparing samples with and without LiF addition sintered at 1400 °C for 5 h, BZCYs/LiF samples were from ~91% to ~96% of the theoretical density, depending on the material, while BZCYs were from ~61% to ~70% dense. Moreover, the appearance and the mechanical properties of the materials are very different when comparing BZCYs/LiF and BZCYs pellets. Comparing the mechanical properties of BZCYs/LiF and BZCYs at similar densities, from different sintering temperatures, pellets with the LiF sintering additive are much tougher than samples without LiF. A hardness test carried out by the Leco microhardness testing system showed that a BZY82/LiF pellet, sintered at 1400 °C for 5 h, had hardness 716.7 HV_{300} and

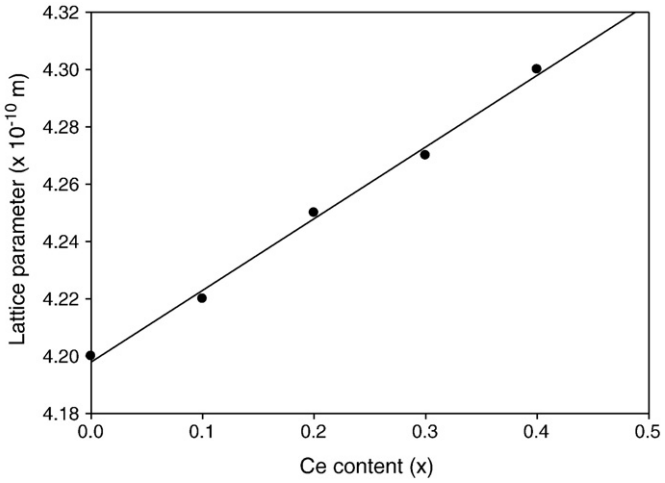

Fig. 2. Pseudo-cubic lattice parameters of BZCYs/LiF.

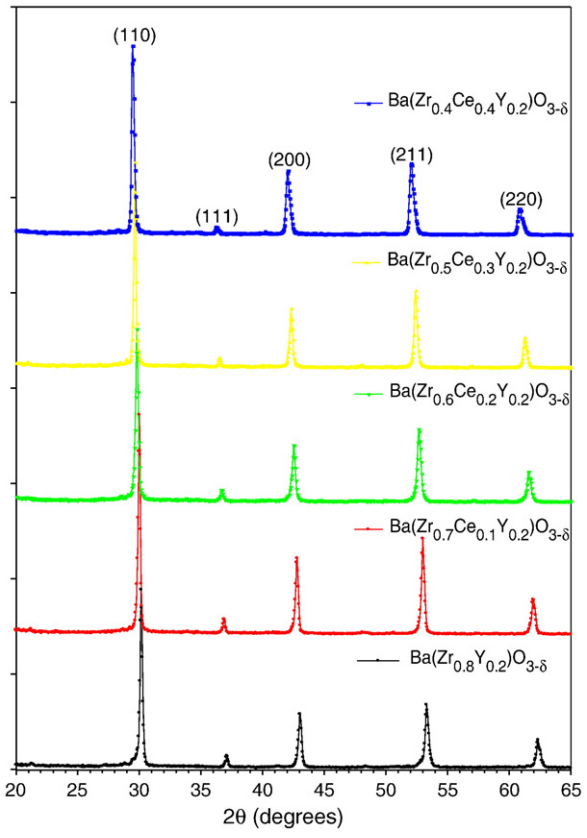

Fig. 1. X-ray diffraction patterns of BZCYs/LiF ceramics which were sintered at 1400 °C for 5 h.

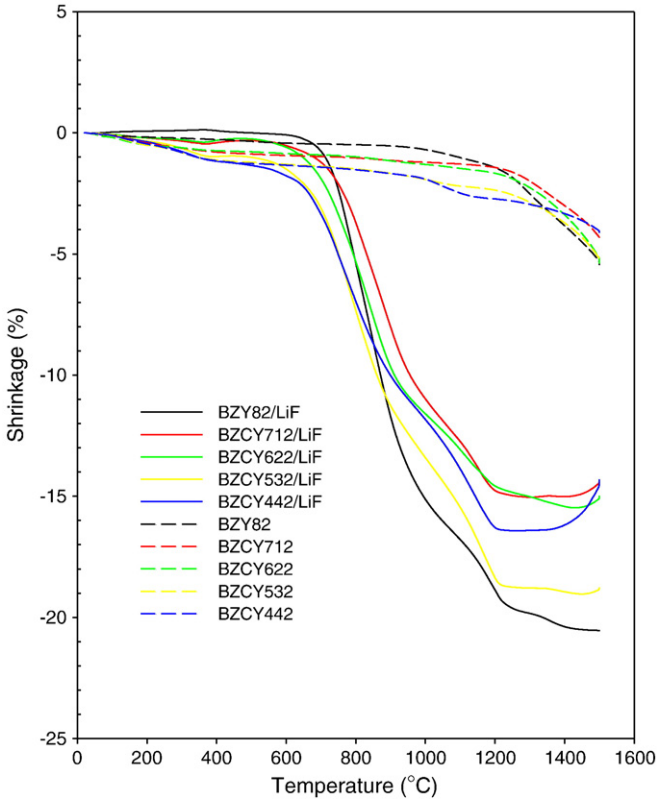

Fig. 3. Temperature dependence of linear shrinkage in BZCYs/LiF and BZCYs.

BZY82, sintered at 1500 °C for 10 h, had hardness 166.0 HV_{300}. The brittleness property of the Y-doped $BaZrO_3$ sample had been reported by many different groups and is a drawback for service as an electrolyte for SOFCs [3,9]. The result of hardness tests shows that this problem can be alleviated considerably by introducing LiF in the sintering process. Another difference is BZCYs disintegrated into small pieces upon exposure to air for a couple of days but BZCYs/LiF stay intact even over a long time of exposure to air. This unique property also shows up in our LiF-added $BaCe_{0.8}Y_{0.2}O_{3-\delta}$ (BCY82/LiF) pellets for electrolyte-supported fuel cells. The BCY82/LiF, ~300 μm thickness, can keep its glossy polished surface after sitting on a desk for more than a year. BCY had been reported highly reactive to CO_2 and H_2O in the air which makes it disintegrate easily upon exposure to air [6,7]. The maximum relative densities that were achieved in the density studies are reported in Table 1.

The reason for the much better mechanical properties for the LiF-added samples is not completely clear, but we can note the following facts. Other workers [3,6,7,9] have make these BZCY ceramics without LiF, using even higher sintering temperatures than we employed, and they also noted poor mechanical properties. Better mechanical properties were achieved by adding zinc oxide, but it was found that zinc reduces the electrical conductivity [19,20]. It seems that without LiF, the grains do not melt together as they should in the sintering process, leading both to low mechanical strength and more opportunity for reaction with air to further lower the strength.

Fig. 4 shows the NRA results from a series of BZCY622 samples which were sintered at 1400 °C with different dwell times. For the as-prepared sample, the two major peaks for lithium and fluorine were identified by the SIMNRA simulation program, Fig. 4(a). After the heat treatment, even without a dwell time at 1400 °C, only a small amount of fluorine was detected by NRA but no lithium was detected in any sintered sample, Fig. 4(b). The results reveal that all the lithium and most of the fluorine evaporated out of the samples during the heating process. Fluorine then continued to leave the samples at a much slower rate at the dwell temperature of 1400 °C. The detection of only fluorine also shows the non-concomitant departure of lithium and fluorine from BZCY622 samples. By integrating the alpha particle spectrum peaks, the amount of fluorine residing in the samples was calculated and shown in Fig. 5. Since fluorine cannot exist inside the sample by itself, this means LiF needs to react with some other material and then decompose to fluoride at a higher temperature. Therefore, a small amount of BZCY622 possibly reacted with LiF as shown in Eq. (6). As temperature increases, Li_2O evaporated gradually from the BZCY622 sample but kept $(Zr,Ce)Y_{0.2}O_{2-\delta}$ inside the structure which made the whole BZCY622 sample a barium deficient system. The $BaLiF_3$ melted incongruently near 850 °C and then decomposed into BaF_2, as seen in Eq. (7).

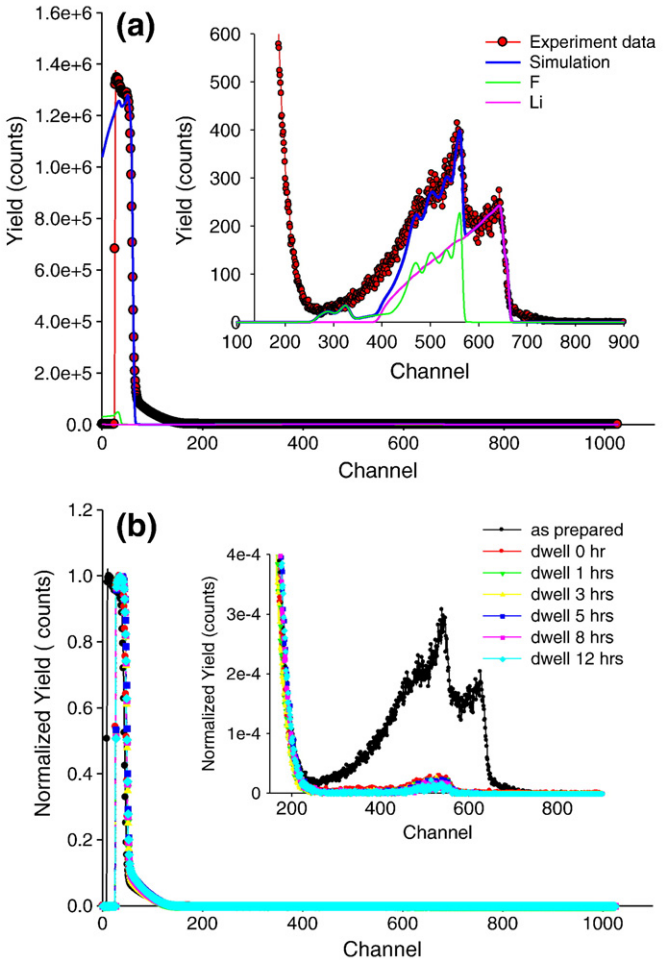

Fig. 4. Nuclear reaction results of (a) as-prepared BZCY622/LiF and SIMNRA simulation of the data and (b) BZCY622/LiF sintered at 1400 °C with dwell time from 0 to 12 h.

$$Ba(Zr_{0.8-x}Ce_xY_{0.2})O_{3-\delta} + 3LiF \rightarrow BaLiF_3 + Li_2O + (Zr,Ce)Y_{0.2}O_{2-\delta} \quad (6)$$

$$BaLiF_3 \rightarrow BaF_2 + LiF. \quad (7)$$

Combining the results above, the liquid phase mixture between LiF, melt point at 848 °C, and $BaLiF_3$, melt point at 857 °C, helps

Table 1
Porosities and the maximum relative densities achieved from densification studies of (a) BZCYs with LiF sintering additive and (b) BZCYs.

	Sintering temperature (°C)	Dwell time (h)	Theoretical density (g/cm^3)	Open porosity (%)	Closed porosity (%)	Relative density (%)
(a) Sample (LiF addition)						
BZY82	1400	5	6.26	1.54	5.83	92.63
BZCY712	1500	8	6.37	1.89	6.92	91.19
BZCY622	1400	5	6.48	0.62	6.29	93.09
BZCY532	1400	5	6.60	1.19	3.96	94.85
BZCY442	1400	5	6.71	0.34	3.66	96.00
(b) Sample						
BZY82	1500	8	6.26	11.53	3.59	84.88
BZCY712	1500	20	6.37	4.33	4.52	91.15
BZCY622	1500	20	6.48	1.63	5.06	93.30
BZCY532	1500	20	6.60	3.78	7.19	89.03
BZCY442	1500	20	6.71	7.20	6.40	86.39

*Theoretical density calculated from XRD results using pseudo-cubic structure and $Ba(Zr_{1-x}Ce_xY_{0.2})O_{2.9}$ as atomic weight formula.

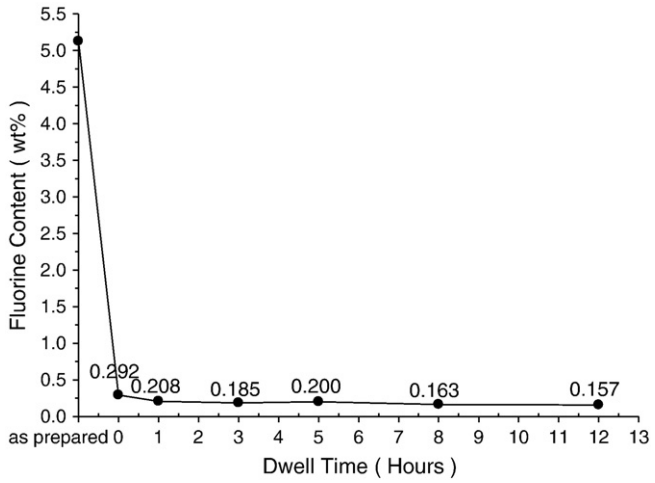

Fig. 5. The amount of fluorine residing inside BZCY622 as a function of dwell time at 1400 °C.

BZCY622 particles to diffuse leading to densification at a lower temperature than when only BZCY622 is used by itself. The solid to liquid phase transformation and diffusion process also explain the fastest sintering mechanism observed in the dilatometry measurement.

Fig. 6 shows the FE-SEM images of BZCYs/LiF which were sintered at 1400 °C with a 5 h dwell time. All the pellets showed a dense structure together with bimodal grain sizes after the sintering process. Roughly half of the volume of BZY82/LiF had micro-size grains (1–2 μm) and the other half had smaller grain sizes (~100 nm). This structure is similar to T. Schober's report in $BaZr_{0.9}Y_{0.1}O_{3-\delta}$ which was sintered at 1715 °C with a 30 h dwell time [12]. As the Ce content increases, the structure maintains its bimodal nature but both large and small grains grew into micrometer sizes. Therefore, the results suggest that the grains grow larger with increasing Ce content in the oxide. Along with the microstructure investigation, an Energy-Dispersive X-Ray Spectrometer (EDS) was used to analyze the chemical composition in both the grain and grain boundary to locate the residual fluorine. However, the fluorine peak was not observed in the spectra due to the small quantity of fluorine present. This is because more fluoride may have evaporated from the sample surface during the thermal etching process and the protecting film in front of the detector blocks out the X-ray signal from lithium, if there is any lithium, and most of the signal from fluorine.

Arrhenius plots of temperature dependent total electrical conductivities with different Ce content in water saturated ($P_{H2O} = 3.5$ kPa) 4% H_2/96% Ar atmosphere are shown in Fig. 7. The inset shows the Ce content versus total conductivities which were measured at 700 °C for BZCYs/LiF and BZCYs. The total conductivities appear with two different slopes at low and high temperature ranges with a separating point ~550 °C. This change of slope at high temperature was attributed to loss of protons, e.g. the dehydration process, in materials at elevated temperature [11,12]. At high temperature, ~550 °C and above, the introduction of Ce into the BZY structure clearly increases the total conductivity. However, the total conductivities of BZCYs/LiF with less than 20% Ce dopant only increased slightly even though the grain size of BZCY622 has increased greatly due to the introduction of Ce. Comparing to BZCYs specimens, individual BZCYs/LiF have higher conductivities than those of BZCYs, except BZCY712/LiF and BZCY712 have similar total conductivity. Although the reason for this increase in conductivity is not clear, a possibility is that the accumulation of BaF_2 along the grain boundary gives a better conductive mechanism, assuming BaF_2 can't go into the perovskite structure because of the different structure. The other possibility could be the deficiency of Ba in the BZCYs/LiF, where LiF takes over Ba from BZCYs to form BaF_2, and increases the proton conductivity. The deficiency of A-site cation in Y-doped ABO_3 resulting in higher total conductivity has been reported by Ma et al. in Y-doped barium cerate and Ferreira et al. in Y-doped strontium zirconia systems [4,25]. According to NRA results, assuming all fluorine which resided inside BZCY622/LiF was in the form of BaF_2, the reaction leads to 2.22 and 1.55 mol% of barium deficiency in BZCY622/LiF which have dwell times of zero and 5 h respectively at 1400 °C. This small amount of BaF_2 is also the reason that we did not see any second phase in XRD spectra. However, the impact of barium deficiency on the electrical property of doped perovskites has not been clarified. In a barium deficient system, Haile et al. proposed that B-site dopant incorporates to A-site, which consumes oxygen vacancies in the material, leading to a dramatic reduction in the conductivity [4]. Ma et al. proposed that deficiency of Ba leaving Ba^{2+}-sites as cation vacancies increases oxygen vacancy concentration and results in higher conductivity [4]. In our experiments, LiF was added after the single phases of BZCYs were obtained. It is more likely that LiF takes over some Ba from BZCY and leaves some Ba^{2+}-sites as cation vacancies. This procedure then gives us higher total conductivities of BZCYs/LiF samples. Another possible simple reason could be that the higher density of LiF-added pellets gave better proton transport which is similar to the better results that often come from higher density pellets sintered at elevated temperature with long soaking time. For example, K. Nomura et al. reported a 96% relative density for BZY82 sintered at 1675 °C for 10 h and measured a total conductivity of 4.2×10^{-3} S/cm at 600 °C in wet 40% H_2–60% Ar atmosphere which is similar to the total conductivity of BZY82/LiF, 3.46×10^{-3} S/cm, at 600 °C in wet 4% H_2–96% Ar atmosphere [13]. Among the three reasons mentioned above, the argument for a slight deficiency of barium in the structure is the favored explanation from our point of view.

At temperatures lower than 350 °C, the impedance spectra can be analysis by ZView software and different semicircles corresponding to grain interior, grain boundary and electrode response can be assigned. Due to the limitation of our facility, grain interior semicircles can only be seen at temperatures below 225 °C. The values for grain interior above 225 °C were taken to be the intercepts of the grain boundary semicircle and the real (Z′) impedance axis. Fig. 8(a) shows the temperature dependent grain interior conductivities of BZCYs/LiF. The inset at the left corner lists the activation energies, E_a, and pre-exponential factors, A, determined from a fit of the data to the Arrhenius equation

$$\sigma = A\exp\left(\frac{-E_a}{k_b T}\right). \tag{8}$$

Among the materials, BZY82/LiF has the highest grain interior conductivity with lowest activation energy. With the increase of Ce content, the grain interior conductivities decrease with an accompanying increase of activation energy. This behavior is consistent with Kreuer's report that $BaZrO_3$ should be a better proton conductor than $BaCeO_3$ by studying the quantum molecular dynamics [3]. For the grain boundary conductivities, samples with Ce content below 20% have similar proton conductivities and then increase the value when Ce content gets higher. If we take the geometry (effective length and area) of grain boundary into account, i.e. specific grain boundary conductivity [9], the value of grain boundary conductivities is about 2 orders of magnitude lower than the data shown in Fig. 8(b). This means that the total resistances of the BZCYs/LiF are more from grain boundary contributions than from the grain interior, which provides the information that the grain boundaries in perovskite BZCYs/LiF are not the favored pathways for fast proton transport at low temperature. Comparing the conductivity measurements between BZCYs/LiF to BZCYs, the activation energies of the grain interior are similar but yet about 0.065 eV higher for the grain boundary, which suggests that the barium deficiency should be small, and the impurity, BaF_2, has accumulated along the grain boundary.

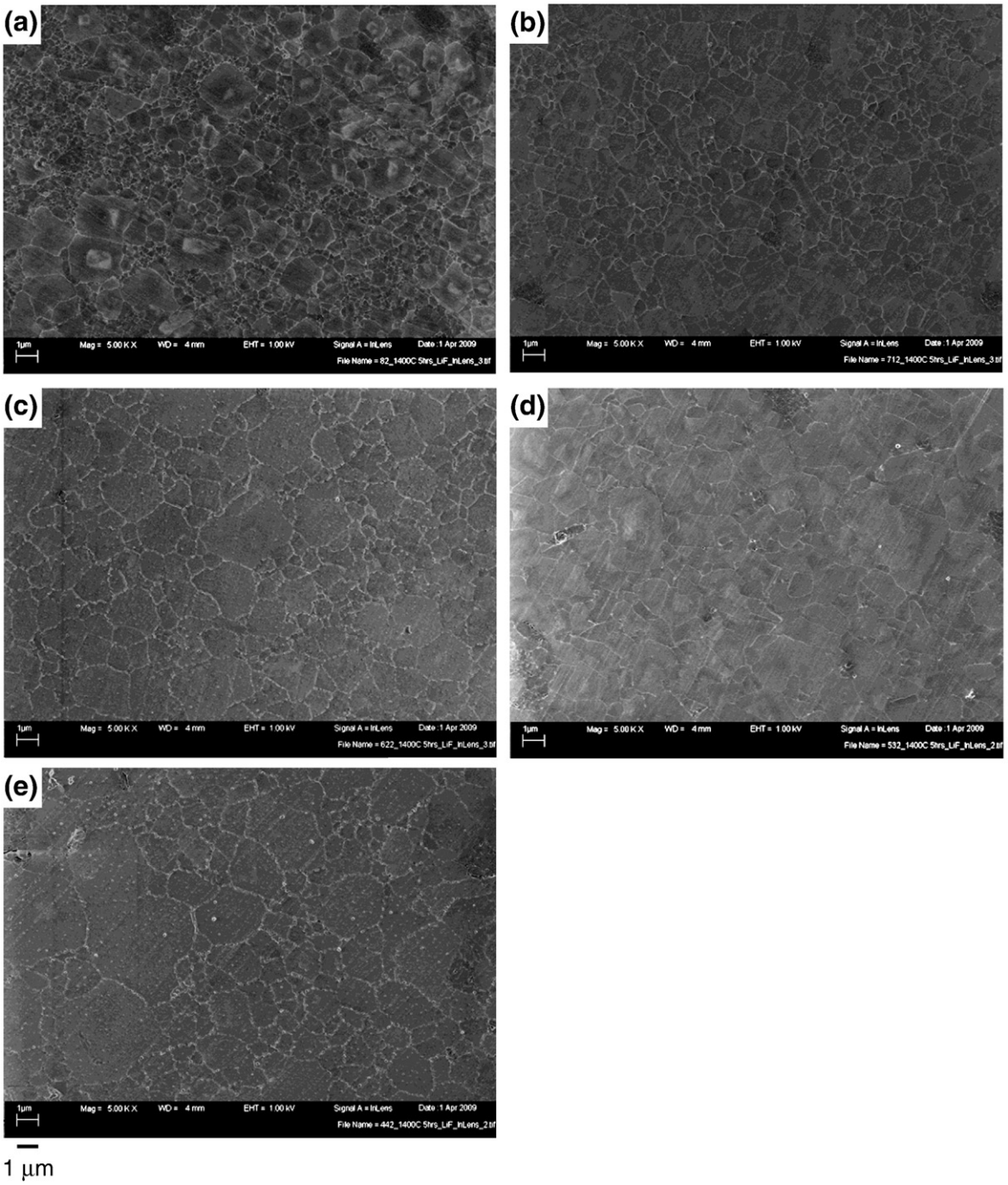

Fig. 6. FE-SEM surface micrograph of sintered (a) BZY82, (b) BZCY712, (c) BZCY622, (d) BZCY532 and (e) BZCY442 at 1400 °C for 5 h.

I–V curves and power densities of electrolyte-supported Pt|BZCYs/LiF|Pt solid oxide fuel cells tested in 800 °C are shown in Fig. 9(a) and 500–850 °C temperature dependent maximum power outputs are shown in Fig. 9(b). The maximum power outputs increase with increasing Ce content of the electrolyte. The tendencies of the temperature dependent power output are consistent with the BZCYs/LiF total conductivity measurements at high temperature. The power outputs of BZCYs/LiF cells are relatively low in our tests. Although the low power output might result from the contribution of polarization between the Pt electrode and BZCYs/LiF electrolytes, the total conductivity measurements do indicate that the total conductivities of BZCYs/LiF are lower than 8 mol% Y-doped zirconia (8YSZ) at temperatures higher than 600 °C. This suggests that a higher amount of Ce must be introduced into the material to produce a comparable power output to the 8YSZ fuel cell at temperature higher than 600 °C. However, a higher Ce content lowers the chemical stability of the fuel cell. For long term tests, all Pt|BZCYs/LiF|Pt cells show stable power outputs for more than 100 h of testing, suggesting that ceramics are very stable under H_2/N_2-air test environments. To get a good power output, a good microstructure design anode supported cell is necessary when BZCYs/LiF are used as the electrolyte membrane in the SOFC.

4. Conclusions

Single phase $Ba(Zr_{0.8-x}Ce_xY_{0.2})O_{3-\delta}$ $(0 \leq x \leq 0.4)$ powders were synthesized by the Glycine-Nitrate Process. By introducing LiF sintering additive, the liquid phase of LiF and its product, $BaLiF_3$,

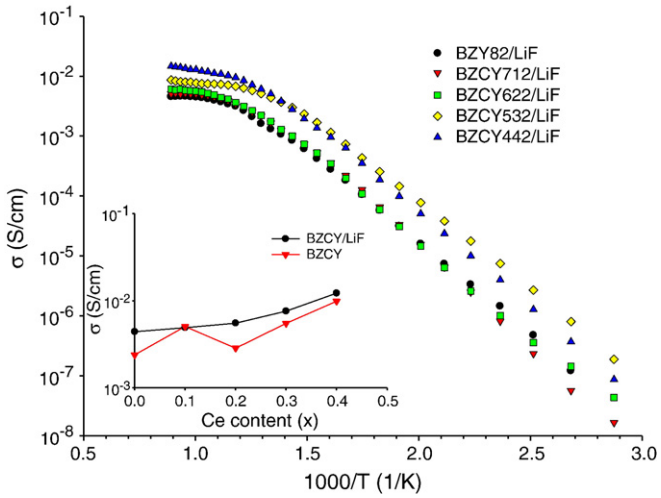

Fig. 7. Total conductivity of BZCYs/LiF as a function of temperature plotted in Arrhenius form. The inset compares the total conductivity of BZCYs/LiF and BZCYs at 700 °C.

melt incongruently around 850 °C which encourages the diffusion between BZCYs particles and results in high density ceramics at reduced sintering temperature (1400 °C) and soaking time (5 h). The mechanical properties and stability of BZCYs are also improved by introducing LiF sintering additive. Nuclear reaction studies show that there is no lithium and only a small amount of fluorine remains inside

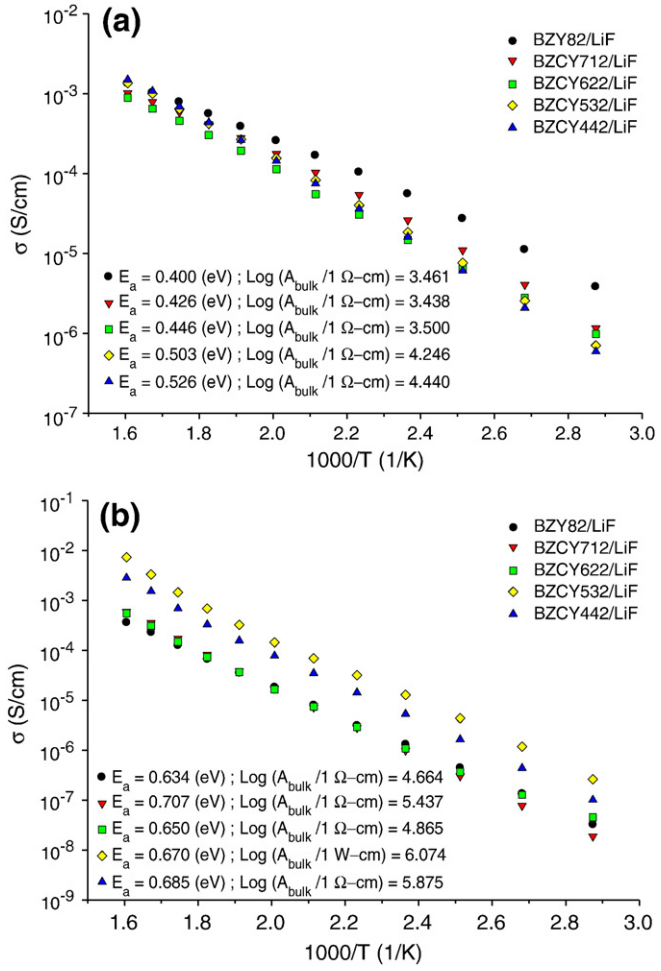

Fig. 8. The conductivity of BZCYs/LiF (a) grain interior conductivity and (b) grain boundary conductivity. The insets show the activation energy and pre-exponential factor of the grain interior and grain boundary respectively.

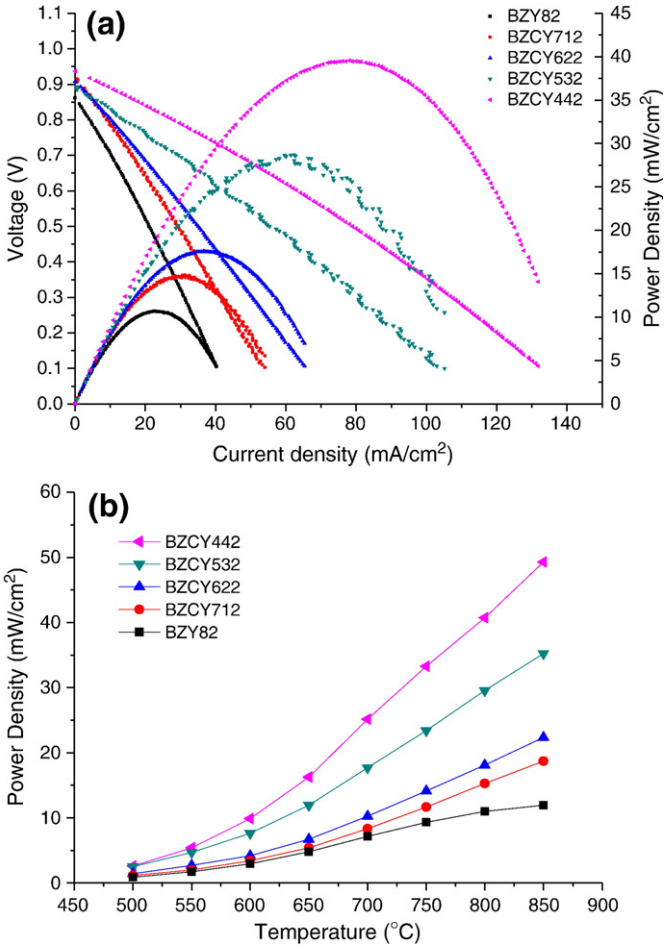

Fig. 9. BZCYs/LiF electrolyte-supported fuel cell with platinum electrodes (a) I–V curves and power density outputs and (b) temperature dependence of maximum power outputs.

the BZCY622/LiF samples which indicates the non-concomitant departure of lithium and fluorine. The slightly higher activation energy at the grain boundary of BZCYs/LiF than that of BZCYs implies fluoride accumulated along the grain boundary. Bimodal grain size distributions were observed in all BZCYs/LiF sintered pellets by FE-SEM. As Ce content increases, both small and big grains grow into bigger micro-size grains but still keep the bimodal structure. Conductivity measurements show that BZY82/LiF has the highest grain interior conductivity which decreases as Ce content increases. In contrast to that for the grain interior, grain boundary conductivities increase with increasing Ce content. When the geometry of the grain boundary is considered, the specific grain boundary conductivity was much lower than the grain interior conductivity, which indicates that the grain boundary is not the favored pathway for proton transport. Compared to BZCYs, individual BZCYs/LiF have higher total conductivities at high temperature than BZCYs which is likely the result of LiF causing a slight barium deficiency in the structure. The fuel cell tests resulted in low power outputs. However, the long term fuel cell tests did show the stable property of BZCYs/LiF ceramics. Overall, LiF is a good sintering additive for sintering BZCYs at lower temperature and makes BZCYs good candidates for serving as electrolytes in sensors and fuel cells.

Acknowledgements

The authors thank Dr. Stephen W. Sofie for the use of all his facilities. This work was supported by the United States Department of Energy, as

a subcontract from Battelle Memorial Institute and Pacific Northwest National Laboratory under Award No. DE-AC06-76RL01830.

References

[1] H. Iwahara, T. Esaka, H. Uchida, N. Maeda, Solid State Ionics (1981) 359 ¾.
[2] H. Iwahara, Solid State Ionics 77 (1995) 333.
[3] K.D. Kreuer, Annu. Rev. Mater. Res. 33 (2003) 333.
[4] G. Ma, T. Shimura, H. Iwahara, Solid State Ionics 110 (1998) 103.
[5] W. Suksamai, I.S. Metcalfe, Solid State Ionics 178 (2007) 627.
[6] B.R. Sneha, V. Thangadurai, J. Solid State Chem. 180 (2007) 2661.
[7] S.V. Bhide, A.V. Virkar, J. Electrochem. Soc. 146 (1999) 2038.
[8] H. Iwahara, H. Uchida, K. Ogki, J. Electrochem. Soc. 135 (1988) 529.
[9] S.M. Haile, G. Staneff, K.H. Ryu, J. Mater. Sci. 36 (2001) 1149.
[10] A. Magrez, T. Schober, Solid State Ionics 175 (2004) 585.
[11] H.G. Bohn, T. Schober, J. Am. Ceram. Soc. 84 (2000) 768.
[12] T. Schober, H.G. Bohn, Solid State Ionics 127 (2000) 351.
[13] K. Nomura, H. Kageyama, Solid State Ionics 178 (2007) 661.
[14] C.-S. Tu, R.R. Chien, V.H. Schmidt, S.-C. Lee, C.-C. Huang, C.-L. Tsai, J. Appl. Phys. 105 (2009) 103504.
[15] E. Fabbri, A. D'Epifanio, E.D. Bartolomeo, S. Licoccia, E. Tracersa, Solid State Ionics 179 (2008) 558.
[16] Z. Zhong, Solid State Ionics 178 (2007) 213.
[17] K.H. Ryu, S.M. Haile, Solid State Ionics 125 (1999) 355.
[18] K. Katahira, Y. Kohchi, T. Shimura, H. Iwahara, Solid State Ionics 138 (2000) 91.
[19] A. D'Epifanio, E. Fabbri, E. Di Bartolomeo, S. Licoccia, E. Traversa, Fuel Cell 08 (2008) No. 1 69.
[20] S. Tao, T.S. Irvine, Adv. Mater. 18 (2006) 1581.
[21] P. Babilo, S.M. Haile, J. Am. Ceram. Soc. 88 (2005) 2362.
[22] M. Pollet, S. Marine, J. Eur. Ceram. Soc. 23 (2003) 1925.
[23] J.M. Haussonne, G. Desgardin, Dielectr. Ceram. (1992) 155.
[24] L.-H. Cao, X.Y. Yao, Z. Xu, Z.-R. Li, Integr. Ferroelectr. 74 (2005) 13.
[25] A.A. Ferreira, J.A. Labrincha, J.R. Frade, Solid State Ionics 77 (1995) 210.